Yellow-Orange-Emitting $CaAlSiN_3:Ce^{3+}$ Phosphor: Structure, Photoluminescence, and Application in White LEDs

Y. Q. Li,* N. Hirosaki, R. J. Xie, T. Takeda, and M. Mitomo

Nitride Particle Group, Nano Ceramics Center, National Institute for Materials Science, Namiki 1-1, Tsukuba, Ibaraki 305-0044, Japan

Received June 18, 2008. Revised Manuscript Received September 17, 2008

The crystal structure and photoluminescence properties of undoped and Ce^{3+}-doped $CaAlSiN_3$ as well as the application of white-light LEDs are reported. $CaAlSiN_3$ and $CaAlSiN_3:Ce^{3+}$ have been synthesized, starting from Ca_3N_2, AlN, Si_3N_4, and CeN or CeO_2 with and without Li_3N, by a solid state reaction at 1700 °C for 4 h under high purity nitrogen atmosphere. Instead of an ideal $CaAlSiN_3$, a more appropriate formula is proposed to be $CaAl_{1-4\delta/3}Si_{1+\delta}N_3$ ($\delta \approx 0.3-0.4$) with an Al/Si ratio of about 1:2 on the basis of the bond valence sum calculations, in which Al/Si is disorderly occupied on the 8b site within $Cmc2_1$ space group. Ce^{3+} can be incorporated into the host lattice of $CaAlSiN_3$, and the estimated maximum solubility of Ce^{3+} is about $x = 0.02$ (e.g., 2.0 mol % with respect to Ca) of $Ca_{1-2x}Ce_xLi_xAlSiN_3$. $CaAlSiN_3:Ce^{3+}$ can be efficiently excited by blue light (450−480 nm) and yields yellow-orange emission with a broadband peaking in the range of 570−603 nm, originating from the $5d^1 \rightarrow 4f^1$ transition of Ce^{3+}. With an increase of Ce concentration, the emission band of Ce^{3+} shifts to longer wavelengths due to the increased Stokes shift corresponding to structural relaxation and energy transfer of Ce^{3+}. Upon excitation in blue light range (450−480 nm), the absorption and external quantum efficiency are about 70% and 56%, respectively, for both $Ca_{1-2x}Ce_xLi_xAlSiN_3$ and $Ca_{1-x}Ce_xAlSiN_{3-2x/3}O_{3x/2}$ at $x = 0.01$. In addition, $Ca_{1-2x}Ce_xLi_xAlSiN_3$ and $Ca_{1-x}Ce_xAlSiN_{3-2x/3}O_{3x/2}$ show high thermal stability in air with the quenching temperature above 300 °C for $x = 0.01$. Using single $CaAlSiN_3:Ce^{3+}$ as the wavelength conversion phosphor combined with a blue InGaN LED-chip (450 nm), warm white-light LEDs can be generated, yielding the luminous efficacy of about 50 lm/W at color temperature 3722 K and the color rendering index (Ra) of 70, which demonstrates that $CaAlSiN_3:Ce^{3+}$ is a highly promising yellow-orange phosphor for use in white-light LEDs.

1. Introduction

With the development of white-light LEDs, in particular for general illumination applications, rare-earth doped silicon nitride based materials have turned out to be the best candidate phosphors for optical wavelength conversion due to their high absorption and conversion efficiency from near-UV to blue spectral region. In addition, with high rigid host lattice, metal silicon nitride based phosphors, in particular for those having three-dimensional framework compounds with corner-sharing (Si, Al)-$(N, O)_4$ tetrahedra and with the ratio of M/Si or M/(Si, Al) ≤ 0.5 (M = alkaline earth metal), normally give a small Stokes shift and good thermal stability (i.e., high thermal quenching temperature).[1−6] Eu^{2+}-actived $CaAlSiN_3$ [5,6] is a newly developed Eu^{2+} red-emitting phosphor for white LED applications after $M_2Si_5N_8:Eu^{2+}$ (M = Ca, Sr, Ba) and has been extensively investigated in recent years.[5−11]

$CaAlSiN_3$ is isostructural with ASi_2N_3 (A = Li, Na) having $Cmc2_1$ space group,[5,7] in which the Ca atom has one crystallographic site at 4a, locating at the channels built up by the six-membered rings of the (Si, Al)N_4 tetrahedra and directly coordinated by nitrogen atoms with a lower coordination number (CN = 5) cross over the unit cell in the range of 2.8 Å. The Si and Al atoms were suggested to be randomly occupied on the 8b site in equivalent. Further, under excitation in the UV and blue visible range, $CaAlSiN_3:Eu^{2+}$ gives a broadband emission with a maximum between 630 and 680 nm, and the optimized Eu concentration is about 1.6 mol %.[5,6] Similar to $M_2Si_5N_8:Eu^{2+}$ (M = Ca, Sr, Ba),[2,3] the emission band shifts toward longer wavelength with increasing Eu^{2+} concentration, corresponding to its body color changing from pale orange to deep red. Upon excitation at 460 nm, the external quantum efficiency reaches up to

* Corresponding author. E-mail: li.yuanqiang@nims.go.jp. Fax: +81-29-851-3613.

(1) Hintzen, H. T.; van Krevel, J. W. H.; Botty, G. European Patent EP-1104 799 A1, 1999.
(2) Höppe, H. A.; Lutz, H.; Morys, P.; Schnick, W.; Seilmeier, A. *J. Phys. Chem. Solids* **2000**, *61*, 2001.
(3) Li, Y. Q.; van Steen, J. E. J.; van Krevel, J. W. H.; Botty, G.; Delsing, A. C. A.; DiSalvo, F. J.; de With, G.; Hintzen, H. T. *J. Alloys Compd.* **2006**, *417*, 273.
(4) Hirosaki, N.; Uheda, K.; Yamamoto, H. PCT WO 2005/052087A1, 2005.
(5) Uheda, K.; Hirosaki, N.; Yamamoto, Y.; Naito, A.; Nakajima, T.; Yamamoto, H. *Electrochem. Solid-State Lett.* **2006**, *9*, 4.
(6) Uheda, K.; Hirosaki, N.; Yamamoto, Y. *Phys. Status Solidi A* **2006**, *203* (11), 2712.
(7) Ottinger, F. Ph.D. Thesis, Universität Karlsruhe, Karlsruhe, 2004.
(8) Mikami, M.; Uheda, K.; Kijima, N. *Phys. Status Solidi A* **2006**, *203* (11), 2705.
(9) Xie, R.-J. In *Phosphor Handbook*, 2nd ed.; Yen, W.; Shionoya, S.; Yamamoto, H., Eds.; CRC Press: Boca Raton, FL, 2007.
(10) Li, J.; Watanabe, T.; Wada, H.; Setoyama, T.; Yoshimura, M. *Chem. Mater.* **2007**, *19* (15), 3592.
(11) Piao, X.; Machida, K.; Horikawa, T.; Hanzawa, H.; Shimomura, Y.; Kijima, N. *Chem. Mater.* **2007**, *19* (18), 4592.

10.1021/cm801669x CCC: $40.75
Published on Web 10/21/2008

~85% at room temperature; moreover, $CaAlSiN_3:Eu^{2+}$ has high thermal stability, just showing a slight decrease up to 160 °C remaining ~87% initial emission intensity at room temperature.[5,6] Both the excitation and emission bands of Eu^{2+} are present in very lower energies due to the contributions by a combination of strong crystal-field splitting of the 5d states of Eu^{2+} and high covalency (nephelauxetic effect), in particular for the first nearest coordination of Eu−N. Additionally, with regard to the synthetic approaches, apart from the traditional solid state reaction at high temperature, $CaAlSiN_3:Eu^{2+}$ also can be prepared by other methods at relative low temperature.[10,11] Combined with other phosphors, $CaAlSiN_3:Eu^{2+}$ has already been successfully applied for white LEDs; for example, for $CaAlSiN_3:Eu^{2+}$ blending with β-Sialon:Eu^{2+} (green) and Ca-α-Sialon:Eu^{2+} (yellow) embedded in a blue-LED chip, white LED yields the color render index (CRI-Ra) of about 80.[12] Furthermore, the CRI-Ra can be increased up to 96 when JEM:Ce^{3+} ($La_{1-x}Ce_x(Si_{6-z}Al_z)N_{10-z}O_z$, blue-green) phosphor is added to the above three kinds of phosphors combined with a UV-LED.[12,13]

In comparison with the Eu^{2+} ion, the Ce^{3+} ion is very simple with just one electron in its excited configuration, that is, $5d^1$. Similarly, the electron within the 5d orbital of the excited Ce^{3+} ion is also strongly dependent on the host lattice, in particular on the local structure. It is believed that the 5d electron can also take part in the formation of the chemical bonds at the excitation state between Ce−N in $CaAlSiN_3$; thus, the lowest 5d excitation bands of Ce^{3+} could be also occurring at longer wavelengths (i.e., lower energies), as found in the case of $M_2Si_5N_8:Ce^{3+}$ (M = Ca, Sr, Ba),[14] which provides more options for use in white-light LEDs. On the other hand, although the crystal structure of $CaAlSiN_3$ is already clear, the distribution of Al/Si is not fully studied apart from the knowledge of its disordering. Therefore, in the present work we report the synthesis, the improved crystal structure, and the photoluminescence properties of undoped and Ce^{3+}-doped $CaAlSiN_3$ as well as the thermal quenching behaviors with an emphasis on the relationship between the crystal structure and photoluminescence properties. Finally, $CaAlSiN_3:Ce^{3+}$ is applied for white-light LEDs integrated with an InGaN based blue-LED chip (450 nm), and the optical characteristics are presented.

2. Experimental Section

Preparation of Binary Cerium Nitride (CeN). Cerium nitride was synthesized by nitridiation of small pieces of Ce metal (Shin-Etsu Chemical Co., Ltd., purity 99%) in a molybdenum crucible at 600−800 °C for 8−12 h under a high purity nitrogen atmosphere in a horizontal tube furnace for firing twice with an intermediate grounding in between. All the processes before and after firing were manipulated in a dried nitrogen-filled glovebox.

Synthesis of $CaAlSiN_3:Ce^{3+}$. Undoped and Ce^{3+}-doped $CaAlSiN_3$ with the ideal compositions of $Ca_{1-2x}Ce_xLi_xAlSiN_3$ (using Li^+ as the charge compensator, $x \leq 0.05$) and $Ca_{1-x}Ce_xAlSiN_{3-2x/3}O_{3x/2}$ (using oxygen anion for the charge balance, $x \leq 0.02$) were prepared by a solid state reaction. The appropriate amounts of Ca_3N_2 (Cerac, purity 99%), α-Si_3N_4 (UBE, SN-E10, α content ~93%), AlN (Tokuyama Chemical Co., Ltd., F-grade), and Li_3N (Aldrich, purity 99%) as well as CeN or CeO_2 (Shin-Etsu Chemical Co., Ltd., purity > 99.9%) were stoichiometricly mixed and ground in a Si_3N_4 mortar within a dried nitrogen filled glovebox. Thereafter, the powder mixture was transferred into a BN crucible and heated at 1700 °C for 4 h under high-purity nitrogen atmosphere under a pressure of 0.48 MPa. For prevention of the evaporation of lithium, the powder bed of the Si_3N_4−10 wt% AlN mixture was used to cover the small BN crucibles within a big BN crucible.

Characterization of $CaAlSiN_3:Ce^{3+}$. The phase formation and crystal structure were analyzed by the X-ray powder diffraction (XRD) (Rigaku, RINT Ultima-III) with graphite monochromator using Cu Kα radiation ($\lambda = 1.54056$ Å), operating at 40 kV and 40 mA. With regard to the air- and moisture-sensitive binary cerium nitride CeN, the prepared samples were mounted on a special quartz glass holder within a tightly sealed aluminum chamber using mylar film to prevent its oxidation during the measurement in air. The Rietveld refinement was performed by the GSAS package, [15,16] and the XRD data were collected in the range of 10−120° in 2θ by a step-scan mode with a step size of 0.02 and a count time of 10 s per step. The single crystal data of $CaAlSiN_3$[7] was used as an initial model for the refinement. To avoid the orientation of the particles, the powder samples were mounted to a holder by a side-filled method.

The photoluminescence spectra were measured by a fluorescence spectrophotometer (Hitachi, F-4500) at room temperature. The diffused reflection spectrum was conducted by a UV/vis spectrophotometer (JASCO, V-560) using $BaSO_4$ white plate as a standard reference. The quantum efficiency was recorded on an intensified multichannel spectrophotometer (Otsuka Electronics, MCPD-7000) with a 200 W Xe-lamp as an excitation source using white $BaSO_4$ powder as a reference for correction of the absorption. The temperature dependent luminescence measurement was also carried out by the MCPD-7000 machine under excitation at 460 nm from room temperature to 300 °C with a heating rate of 100 °C/min and a holding time of 5 min for each temperature point. The single-phosphor LEDs were fabricated by coating varied amounts of the yellow-orange phosphor of $CaAlSiN_3:Ce^{3+}$ in silicon on an InGaN blue LED chip (~ 450 nm) as the primary light source. The optical properties of LEDs were performed by MCPD-7000 under a forward-bias current of 20 mA at room temperature.

3. Results and Discussion

3.1. Binary Cerium Nitride CeN. Figure 1 shows the powder X-ray diffraction pattern of the obtained cerium nitride compound. It was found that the nitridation reaction was nearly complete after firing twice at the same conditions and the final product can be approximately formulated as $CeN_{0.97}$ determined by the weight-gain method. The presence of a small amount cerium oxynitride (~1%), namely, Ce_2ON_2,[17] may be related to the initial oxygen impurity covered on as-received Ce metal surface. $CeN_{0.97}$ is crystallized in a cubic system (space group *Fm*3*m*), and the refined lattice parameter is $a = 5.0216(1)$ Å, perfectly matching with

(12) Sakuma, K.; Hirosaki, N.; Kimura, N.; Ohashi, M.; Xie, R. J.; Yamamoto, Y.; Seuhiro, T.; Asano, K.; Tanaka, D. *IEICE Trans. Electron.* **2005**, *E88-C*, 2057.
(13) Hirosaki, N.; Xie, R. J.; Sakuma, K. *Bull. Ceram. Soc. Jpn.* **2006**, *41*, 602.
(14) Li, Y. Q.; de With, G.; Hintzen, H. T. *J. Lumin.* **2006**, *116*, 107.
(15) Larson, A. C.; Von Dreele, R. B. Report LAUR 86-748, Los Alamos National Laboratory: Los Alamos, NM, 2000.
(16) Toby, B. H. *J. Appl. Crystallogr.* **2001**, *34*, 210.
(17) Alexander, B. M. *J. Chem. Soc., Dalton Trans.* **1974**, 2166.

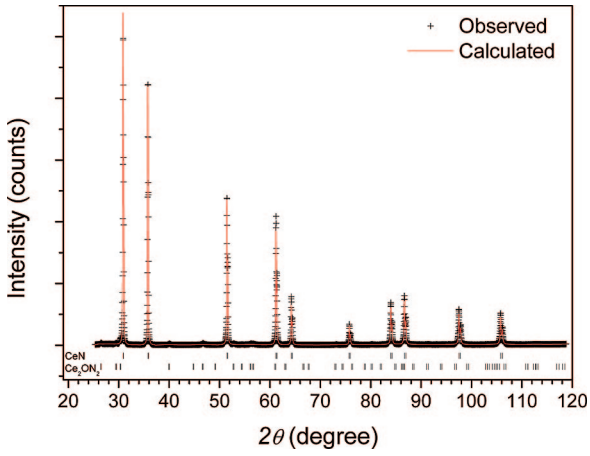

Figure 1. X-ray powder diffraction pattern of $CeN_{0.97}$.

the reported XRD data.[17,18] The indexed powder (using DICVOL04 indexing program[19]) XRD data can be found in the Supporting Information.

3.2. Composition and structural characteristics of $CaAlSiN_3$ and $CaAlSiN_3$:Ce^{3+}. As usual for nitride compounds, the oxygen impurity is unavoidable from the starting materials and from the second contamination in the processing. The total oxygen content of the powdered $Ca_{1-2x}Ce_xLi_xAlSiN_3$ ($x = 0.01$), for example, is about $2.0 \pm 0.1\%$. A higher oxygen content in $Ca_{1-x}Ce_xAlSiN_{3-2x/3}O_{3x/2}$ is expected. Both $Ca_{1-2x}Ce_xLi_xAlSiN_3$ and $Ca_{1-x}Ce_xAlSiN_{3-2x/3}O_{3x/2}$ phosphors show high chemical stability in air, similar to $M_2Si_5N_8$:Ce^{3+}.

Figure 2 shows the Rietveld refinement XRD patterns of $CaAlSiN_3$, $Ca_{1-2x}Ce_xLi_xAlSiN_3$ ($x = 0.01$), and $Ca_{1-x}Ce_xAlSiN_{3-2x/3}O_{3x/2}$ ($x = 0.01$). Under the present synthetic conditions, according to the stoichiometric composition both undoped and Ce^{3+}-doped $CaAlSiN_3$ are hardly obtained in single-phase form with very small amounts of secondary phase, that is, AlN-like for undoped and unidentified for Ce-doped materials (see Figure 2), depending on the overall composition. Both the lattice parameters and the atomic positions are very close to the previously reported crystallographic data.[5−7] However, the distribution of Al/Si markedly varies with the composition and the synthetic methods. Because of very similar scattering factors of Al^{3+} and Si^{4+}, it is impossible to discriminate them with X-ray diffraction as expected. Therefore, the bond valence sum calculations were carried out to check the distribution of disordering Al/Si in $CaAlSiN_3$. Table 1 summarized the calculated bond valence sums [20,21] and the estimated Al/Si ratio of $CaAlSiN_3$ (included reference data from refs 5, 7, and 11), $Ca_{1-2x}Ce_xLi_xAlSiN_3$ ($x = 0.01$), and $Ca_{1-x}Ce_xAlSiN_{3-2x/3}O_{3x/2}$ ($x = 0.01$). Surprisingly, Al/Si is found to be occupied at the 8b site in space group of $Cmc2_1$ with a ratio of about 1/2 by a solid state reaction method in all the cases not 1/1

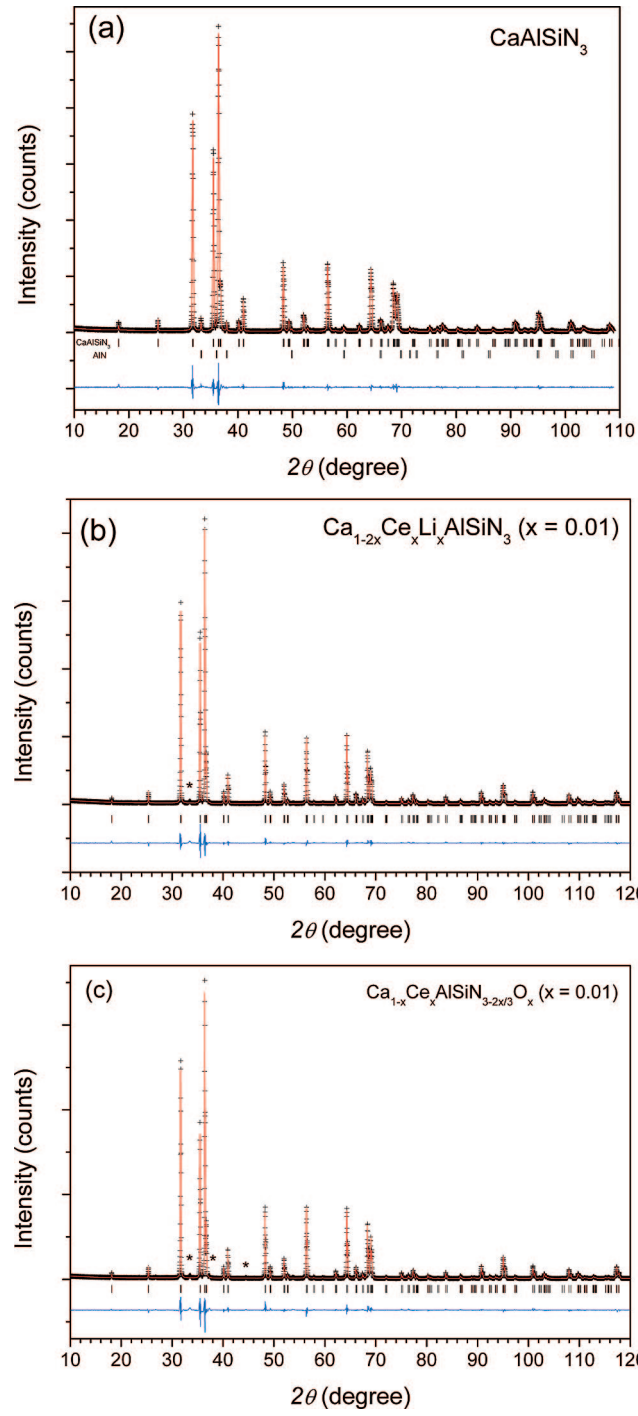

Figure 2. Rietveld refinement X-ray patterns of (a) $CaAlSiN_3$, (b) $Ca_{1-2x}Ce_xLi_xAlSiN_3$ ($x = 0.01$), and (c) $Ca_{1-x}Ce_xAlSiN_{3-2x/3}O_{3x/2}$ ($x = 0.01$). Asterisks indicate the impurity phase.

(i.e., the frictional occupation of 0.5, 0.5 for Al and Si, respectively) as previously proposed for both powder[5] and single crystal[7] compounds. However, a larger derivation (i.e., Al/Si = 0.25/0.75) can also be found by the self-propagating high-temperature synthesis approach[11] indicting that the obtained material is far away from the stoichiometric $CaAlSiN_3$ not only on Al/Si but also on N or N/O, obviously due to its low firing temperatures (1450−1550 °C) and/or incomplete reaction resulting in a significantly lower Al solubility in $CaAlSiN_3$ which is well consistent with its much smaller lattice parameters.[11] Therefore, an approximate composition maybe can be formulated as $Ca_{1-\delta/2}Al_{1-\delta}Si_{1+\delta}N_3$

(18) (a) National Bureau of Standards Monographs; National Bureau of Standards: Gaithersburg, MD, 1966; Vol. 51, p 254. (b) International Center for Diffraction Data, PDF 015-0882.
(19) (a) Boultif, A.; Louer, D. *J. Appl. Crystallogr.* **2004**, *37*, 724. (b) Louer, D.; Louer, M. *J. Appl. Crystallogr.* **1972**, *5*, 271. (c) Boultif, A.; Louer, D. *J. Appl. Crystallogr.* **1991**, *24*, 987.
(20) Brown, I. D.; Altermatt, D. *Acta Crystallogr.* **1985**, *B41*, 244.
(21) Brese, N. E.; O'Keeffe, M. *Acta Crystallogr.* **1991**, *B47*, 192.

Table 1. Bond Valence Sums (BVS) and the Al/Si Distribution in $CaAlSiN_3$ and $CaAlSiN_3:Ce^{3+}$

$CaAlSiN_3$								
	this work		Uhead et al.[5]		Ottinger[7]		Piao et al.[11]	
atom	BVS	Al/Si	BVS	Al/Si ratio	BVS	Al/Si ratio	BVS	Al/Si ratio
Ca	2.039		2.005		1.927		2.123	
Al/Si[a]	3.696(3.835/3.634)	0.31/0.69	3.67 (3.804/3.604)	0.33/0.67	3.63 (3.756/3.558)	0.37/0.63	3.76(3.914/3.708)	0.25/0.75
N1	−3.139		−3.176		−3.138		−3.218	
N2	−3.153		−2.994		−2.913		−3.211	

$CaAlSiN_3:Ce^{3+}$					
$Ca_{0.98}Ce_{0.01}Li_{0.01}Al_{0.6}Si_{1.3}N_3$			$Ca_{0.99}Ce_{0.01}Al_{0.501}Si_{1.374}N_{2.9933}O_{0.015}$		
atom	BVS	Al/Si ratio	atom	BVS	Al/Si ratio
Ca/Ce/Li	1.995		Ca/Ce	2.040	
Al/Si[a]	3.665(3.797/3.597)	0.35/0.65	Al/Si	3.692(3.632/3.827)	0.31/0.69
N1	−3.121		N1/O1	−3.148	
N2	−3.084		N2/O2	−3.122	

[a] The calculated BVS data of Al and Si are given in parenthsis.

Table 2. Atomic and Total MAPLE (kJ/mol) Data for the Two Models of $CaAlSiN_3$

atom	Ca	Al/Si	N1	N2	ΣMAPLE	ΣMAPLE (Ca_3N_2 + AlN + α-Si_3N_4)	ΔMAPLE[a]
$Ca_{1-\delta/2}Al_{1-\delta}Si_{1+\delta}N_3$ ($\delta = 0.38$)	1341.52	8250.05	5592.43	5230.08	34305.74	36729.42	6.6%
$CaAl_{1-4\delta/3}Si_{1+\delta}N_3$ ($\delta = 0.38$)	1680.89	7829.78	5942.73	5664.71	34940.7	36083.60	3.2%

[a] ΔMAPLE: difference in MAPLE data between ΣMAPLE and ΣMAPLE (Ca_3N_2 + AlN + α-Si_3N_4).

or $CaAl_{1-4\delta/3}Si_{1+\delta}N_3$ ($\delta \approx 0.3 - 0.4$) instead of an ideal $CaAlSiN_3$. The Madelung partial lattice energy (MAPLE) [22,23] calculated data (Table 2) suggest that $CaAl_{1-4\delta/3}Si_{1+\delta}N_3$ is more possible than $Ca_{1-\delta/2}Al_{1-\delta}Si_{1+\delta}N_3$ due to a small difference in MAPLE data between $CaAl_{1-4\delta/3}Si_{1+\delta}N_3$ and its MAPLE sums consisting of the binary compounds of Ca_3N_2, AlN, and Si_3N_4 (i.e., ΔMAPLE in Table 2). It is worth noting that the exact δ value in $CaAlSiN_3$, of course, is needed to be further confirmed/refined by neutron diffraction. Meanwhile, a big deviation from −3 of N by the BVS calculations implies that a small amount of unwanted oxygen must have been incorporated into N1 and N2 crystallographic site not only in $CaAlSiN_3$ but also in $CaAlSiN_3:Ce^{3+}$ (Tables 1 and 2), as found in all nitride compounds, in fact. It seems that the more negative the valences of N1 and N2, the larger the amount of oxygen impurity introduced into the lattice, which can readily make a judgment from $Ca_{1-2x}Ce_xLi_xAlSiN_3$ ($x = 0.01$) and $Ca_{1-x}Ce_xAlSiN_{3-2x/3}O_{3x/2}$ ($x = 0.01$) (Table 1). In addition, a very large difference in MAPLE data (i.e., ΔMAPLE = 3.2%) between ΣMAPLE($CaAlSiN_3$) and ΣMAPLE(Ca_3N_2 + AlN + α-Si_3N_4) is observed which probably is related to the formal valence of Ca being in between +1.5 and +2 other than +2 in Ca_3N_2. Exactly the same case, that is, a large ΔMAPLE, is also found in other alkaline-earth silicon nitride compounds, for example, in $Ca_2Si_5N_8$ and $CaSiN_2$ (orthorhombic), where ΔMAPLE reaches about 3% and 6%, respectively. Apart from the valence of Ca of Ca_3N_2, a small amount of oxygen impurity occupied at the N site is also partially responsible for this deviation. From the above discussions, it is understood that both the powder and the single crystal forms hardly reach Al/Si = 1 practically; therefore, it can be easily explained why there is always a small amount of AlN-like secondary phase present in the final compounds following the stoichiometric composition of an ideal $CaAlSiN_3$ in preparations. Structurally, an ideal $CaAlSiN_3$ is very favorable for the luminescent intensity/quantum efficiency of Ce^{3+}- or Eu^{2+}-doped $CaAlSiN_3$ due to an increase of the nearest distance of (Ca, Ce)−(Ca, Ce) or (Ca, Eu)−(Ca, Eu), improving the conversion efficiency and increasing the critical concentration of quenching of the luminescence centers. It should be noted that, for simplicity, we still use the formula of $CaAlSiN_3$ in the whole text.

The final refined crystal structures of $CaAlSiN_3$, $Ca_{1-2x}Ce_xLi_xAlSiN_3$ ($x = 0.01$), and $Ca_{1-x}Ce_xAlSiN_{3-2x/3}O_{3x/2}$ ($x = 0.01$) are summarized in Table 3, and the selected interatomic distances and angles are listed in Table 4. Ce^{3+} can be incorporated into the $CaAlSiN_3$ lattice forming a limited solid solution. As a heterovalent substitution, one Ce^{3+} ion can partially replace one Ca^{2+} ion accompanying Li^+ at the same Ca site for maintaining electronic neutralization of $CaAlSiN_3$, as shown in Figure 3. In summary, the crystallographic data demonstrate that $CaAlSiN_3$ and $CaAlSiN_3:Ce^{3+}$ are not perfect but imperfect structures with partial Al vacancies in $CaAl_{1-4\delta/3}Si_{1+\delta}N_3$ and $CaAl_{1-4\delta/3}Si_{1+\delta}N_3:Ce^{3+}$.

There are no big differences between $CaAlSiN_3$ and $Ca_{1-2x}Ce_xLi_xAlSiN_3$ or $Ca_{1-x}Ce_xAlSiN_{3-2x/3}O_{3x/2}$ in structures, apart from different Al/Si ratio and a slight distortion in the lattices. As a result of a markedly lower Al/Si ratio in undoped $CaAlSiN_3$ (Table 1), the lattice parameters are significantly smaller than that of Ce^{3+},Li^+ codoped $CaAlSiN_3$ because short Si−N (1.65−1.75 Å) is dominance of the (Si, Al)-N bonds other than long Al−N (1.75−1.85 Å).[21,24,25] Obviously, Al/Si ratio is very difficult to reach up to 1, but Li can significantly increase the solubility of Al besides a way of increasing the firing temperature (as in the case of refs 5 and 7) by a solid state reaction approach due to the

(22) Hoppe, R. *Angew. Chem.* **1966**, *78*, 52.
(23) Hoppe, R. *Angew. Chem.* **1970**, *82*, 7.
(24) Trigg, M. B.; Jack, K. H. *J. Mater. Sci. Lett.* **1987**, *6*, 407.
(25) Petzow, G.; Herrmann, M. *Struct. Bonding (Berlin)* **2002**, *102*, 47.

Table 3. Crystal Structure Data and Isotropic Displacement Parameters of $CaAlSiN_3$ and $CaAlSiN_3:Ce^{3+}$ Crystal System[a]

formula	$CaAlSiN_3$ ($CaAl_{0.49}Si_{1.38}N_3$)[b]
density	3.232 (g/cm^3)
lattice parameters	$a = 9.7558(2)$, $b = 5.6473(1)$, $c = 5.0524(1)$, $V = 278.36(1)$
R_{wp}	8.6%
R_p	6.3%
χ^2	3.3

atom	Wyck.	*x/a*	*y/b*	*z/c*	S.O.F.	*U* (100 Å^2)
Ca1	4a	0.0000	0.3154(3)	0.4921(4)	1.00	2.00(1)
(Al, Si)1	8b	0.1723(2)	0.1560(3)	0.0177(1)	0.27/0.69	0.04(1)
N1	8b	0.2120(4)	0.1264(8)	0.3708(6)	1.00	0.08(2)
N2	4a	0.0000	0.2379(7)	−0.0308(13)	1.00	0.04(1)

formula	$Ca_{0.98}Ce_{0.01}Li_{0.01}AlSiN_3$ ($Ca_{0.98}Ce_{0.01}Li_{0.01}Al_{0.6}Si_{1.3}N_3$)[b]
density	3.216 (g/cm^3)
lattice parameters	$a = 9.7950(1)$, $b = 5.6465(1)$, $c = 5.0590(1)$, $V = 279.80(1)$
R_{wp}	8.7%
R_p	6.2%
χ^2	4.0

atom	Wyck.	*x/a*	*y/b*	*z/c*	S.O.F.	*U* (100 Å^2)
(Ca, Ce, Li)1	4a	0.0000	0.3157(3)	0.4946(1)	0.98/0.01/0.01	1.55(1)
(Al, Si)1	8b	0.1721(2)	0.1563(3)	0.0218(4)	0.30/0.65	0.1(1)
N1	8b	0.2122(3)	0.1238(8)	0.3756(5)	1.00	0.3(2)
N2	4a	0.0000	0.2431(7)	−0.0253(11)	1.00	0.34(3)

density	3.218 (g/cm^3)
formula	$Ca_{0.99}Ce_{0.01}AlSiN_{2.9933}O_{0.015}$ ($Ca_{0.99}Ce_{0.01}Al_{0.501}Si_{1.374}N_{2.9933}O_{0.015}$)[b]
lattice parameters	$a = 9.7878(2)$, $b = 5.6465(1)$, $c = 5.0580(1)$, $V = 279.54(1)$
R_{wp}	9.95%
R_p	7.3%
χ^2	4.3

atom	Wyck.	*x/a*	*y/b*	*z/c*	S.O.F.	*U* (100 Å^2)
(Ca, Ce)1	4a	0.0000	0.3150(4)	0.4952(1)	0.99/0.01	1.69(5)
(Al, Si)1	8b	0.1713(2)	0.1563(3)	0.0218(4)	0.25/0.69	0.06(3)
(N, O)1	8b	0.2087(4)	0.1143(10)	0.3738(6)	0.998/0.005	0.29(17)
(N, O)2	4a	0.0000	0.2436(8)	−0.0338(13)	0.998/0.005	0.29(17)

[a] Orthorhombic; space group: $Cmc2_1$ (No. 36); $Z = 4$. Lattice parameters: *a*, *b*, and *c* in Å; *V* in Å^3; S.O.F. = site occupancy fraction. [b] The proposed composition is given in parenthesis.

Table 4. Selected Interatomic Distances (Å) and Angles (deg) of $CaAlSiN_3$ and $CaAlSiN_3:Ce^{3+}$

	$CaAlSiN_3$		$Ca_{0.98}Ce_{0.01}Li_{0.01}AlSiN_3$	$Ca_{0.99}Ce_{0.01}AlSiN_{2.9933}O_{0.015}$
Ca1−N1	2.4066(26) ×2	(Ca, Ce)1−(N, O)1	2.4199(25)× 2	2.415(3) × 2
Ca1−N2	2.678(6)	(Ca, Ce)1−(N, O)2	2.463(6)	2.416(7)
Ca1−N2	2.450(6)	(Ca, Ce)1−(N, O)2	2.493(4)	2.497(5)
Ca1−N2	2.525(4)	(Ca, Ce)1−(N, O)2	2.662(5)	2.706(7)
mean	2.4932	mean	2.4916	2.4898
(Si, Al)1−N2	1.7607(21)	(Si, Al)1−(N, O)2	1.7709(20)	1.7694(22)
(Si, Al)1−N1	1.801(5)	(Si, Al)1−(N, O)1	1.786(4)	1.7430(50)
(Si, Al)1−N1	1.826(5)	(Si, Al)1−(N, O)1	1.841(5)	1.8327(33)
(Si, Al)1−N1	1.8334(33)	(Si, Al)1−(N, O)1	1.8449	1.901(6)
mean	1.8053	mean	1.8107	1.8115
N2−Ca1−N2	160.29(19)	(N, O)2−(Ca, Ce)1−(N, O)2	161.57(18)	161.84(22)
N1−Ca1−N1	118.48(24)	(N, O)1−(Ca, Ce)1−(N, O)1	118.37(23)	115.49(30)
N1−Ca1−N2	115.56(13)× 2	(N, O)1−(Ca, Ce)1−(N, O)2	115.94(13) × 2	116.96(17) × 2
N2−Ca1−N2	102.93(17)	(N, O)2−(Ca, Ce)1−(N, O)2	101.89(16)	102.97 (18)
N1−Ca1−N2	99.86(9)× 2	(N, O)1−(Ca, Ce)1−(N, O)2	99.83(8) × 2	99.94(10) × 2
N2−Ca1−N2	96.79(19)	(N, O)2−(Ca, Ce)1−(N, O)2	96.54(18)	95.90(11)
N1−Ca1−N2	71.11(8) × 2	(N, O)1−(Ca, Ce)1−(N, O)2	71.66(8) × 2	71.25(9) × 2

lower melting point of the Li compounds. The difference between $Ca_{1-2x}Ce_xLi_xAlSiN_3$ and $Ca_{1-x}Ce_xAlSiN_{3-2x/3}O_{3x/2}$ is even small in structures, for example an overall change of the unit cell volume just of about 0.09% for $x = 0.01$. Unlike $CaAlSiN_3:Eu^{2+}$, where Eu^{2+} substitution for Ca^{2+} has the same formal charge and the ionic radius of Eu^{2+} (1.17 Å, CN = 6) is much larger than that of Ca^{2+} (1.00 Å, CN = 6).[26] Therefore, the incorporation of Eu^{2+} leads to a marked expansion of the host lattice.[5,6] However, the ionic radius of Ce^{3+} (1.01 Å, CN = 6)[26] is almost the same with Ca^{2+}. Thus, it is expected that the expansion of the lattice parameters of $CaAlSiN_3:Ce^{3+}$ would be very limited in total

(26) Shannon, R. D. *Acta Crystallogr.* **1976**, *A 32*, 751.

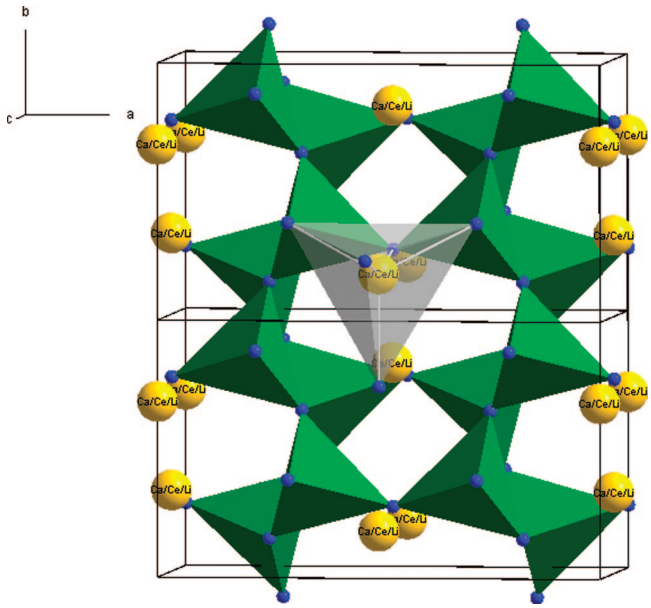

Figure 3. Projection of the crystal structure of $CaAlSiN_3$:Ce, Li, and the local coordination polyhedron of (Ca, Ce, Li)N_5, viewed along [001].

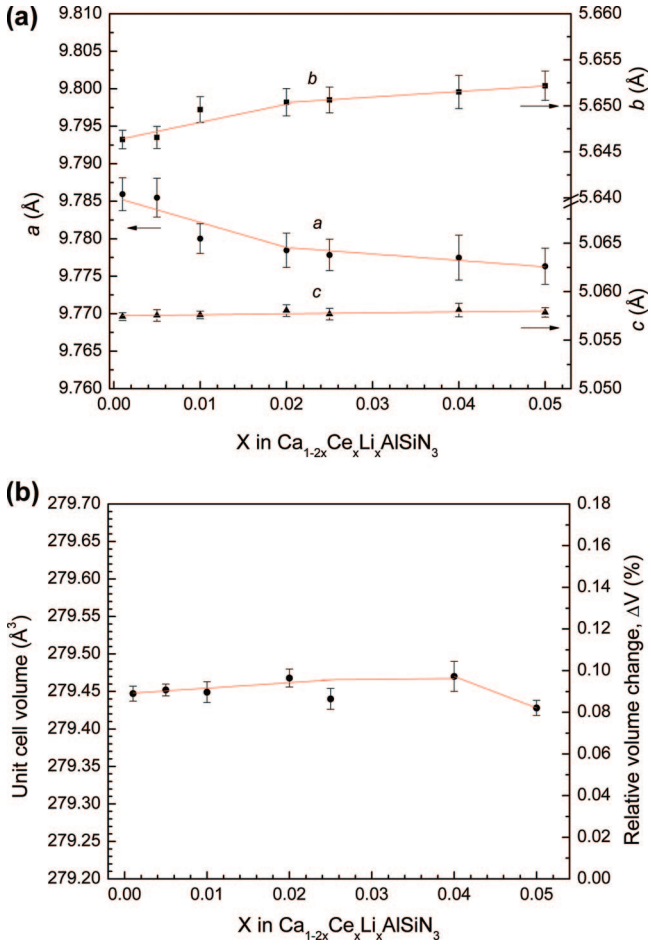

Figure 4. Variation of the lattice parameters of (a) *a*, *b*, and *c* and (b) unit cell volume with *x* of $Ca_{1-2x}Ce_xLi_xAlSiN_3$.

due to the substitution Ce^{3+} for Ca^{2+}. Indeed, the obtained data by XRD demonstrate this is the real case, as shown in Figure 4. With an increase of the Ce^{3+} concentration, say *x*, the *a*-axis slightly decreases with a breaking point at about $x = 0.02$, from which the drop rate decreases slightly. The

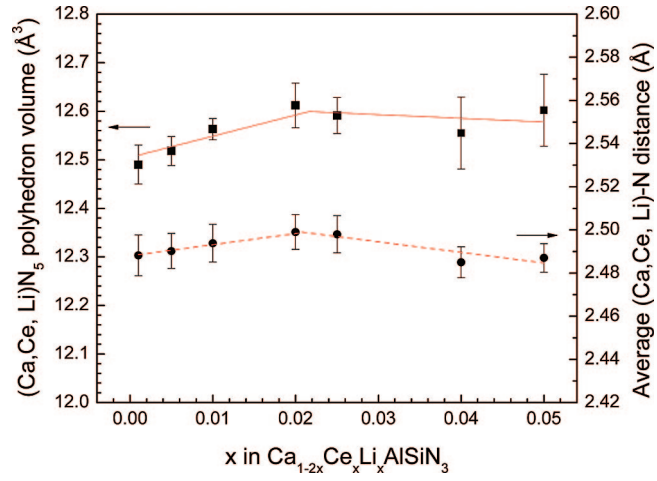

Figure 5. Variations of the polyhedron volume (Ca, Ce, Li)−N_5 and the average distance of (Ca, Ce, Li)−N with *x* in $Ca_{1-2x}Ce_xLi_xAlSiN_3$.

introduction of Li^+ along with Ce^{3+} on the Ca^{2+} site is mainly responsible for this shrinkage because Li^+ (0.76 Å, CN = 6)[26] is much smaller than Ca^{2+}. In contrast, the *b*-axis shows a slight increase with a breaking point at $x = 0.02$. Meanwhile, the *c*-axis almost remains the same, indicating that the lattice is more rigid along the *c*-axis than along the *a*- and *b*-axes (Figure 4a). As a result, the unit cell volume of $CaAlSiN_3$:Ce,Li slightly increases to $x = 0.04$ and then decreases due to more Li replacement of Ca. Actually, the overall change of the unit cell volume is still so small (~0.014% from $x = 0.001$ to 0.05) that it can be regarded as keeping constant (Figure 4b), arising from a counteraction effect of the Li^+ ion particularly along the *a*-axis direction. The same situation is also found in $Ca_{1-x}Ce_xAlSiN_{3-2x/3}O_{3x/2}$, in which with increasing *x* the *a*-axis decrease due to the replacement of N^{3-} (1.46 Å for CN = 4) by O^{2-} (1.35 Å for CN = 4),[26] but the *b*- and *c*-axes increase due to Ce replacement of Ca. With the present situation, unfortunately, it is impossible to exactly determine the maximum solubility of Ce^{3+} in the $CaAlSiN_3$ lattice just by XRD alone. Approximately, a solubility limit seems at the breaking point (Figure 4a), namely, $x = 0.02$ or more. It is further confirm by its local structure changes and their luminescence spectra.

In contrast to the limited expansion of the host lattice, the local structure around (Ca, Ce, Li), namely, the interatomic distance of (Ca, Ce, Li)−N and the coordination polyhedron volume of (Ca, Ce, Li)N_5 with a C_1 point symmetry, has large increase with increasing Ce concentration for $Ca_{1-2x}Ce_xLi_xAlSiN_3$ (Figure 5). The total increments of the (Ca, Ce, Li)N_5 polyhedron volume and (Ca, Ce, Li)−N distance are about 1.23% and 0.5%, respectively, which are markedly larger than the overall volume change of the lattice (~0.014%), suggesting that the local lattice relaxation around Ce has a larger contribution to the luminescence properties of Ce^{3+} than that of the average structural change. As same as the *a*- and *b*-axes, both the (Ca, Ce, Li)N_5 polyhedron volume and the mean (Ca, Ce, Li)−N distance show a decreased tendency when *x* is above 0.02 for $Ca_{1-2x}Ce_xLi_xAlSiN_3$; thus, the interatomic distances, for example, (Ca, Ce, Li)−N and the nearest Ce−Ce, are decreased correspondingly.

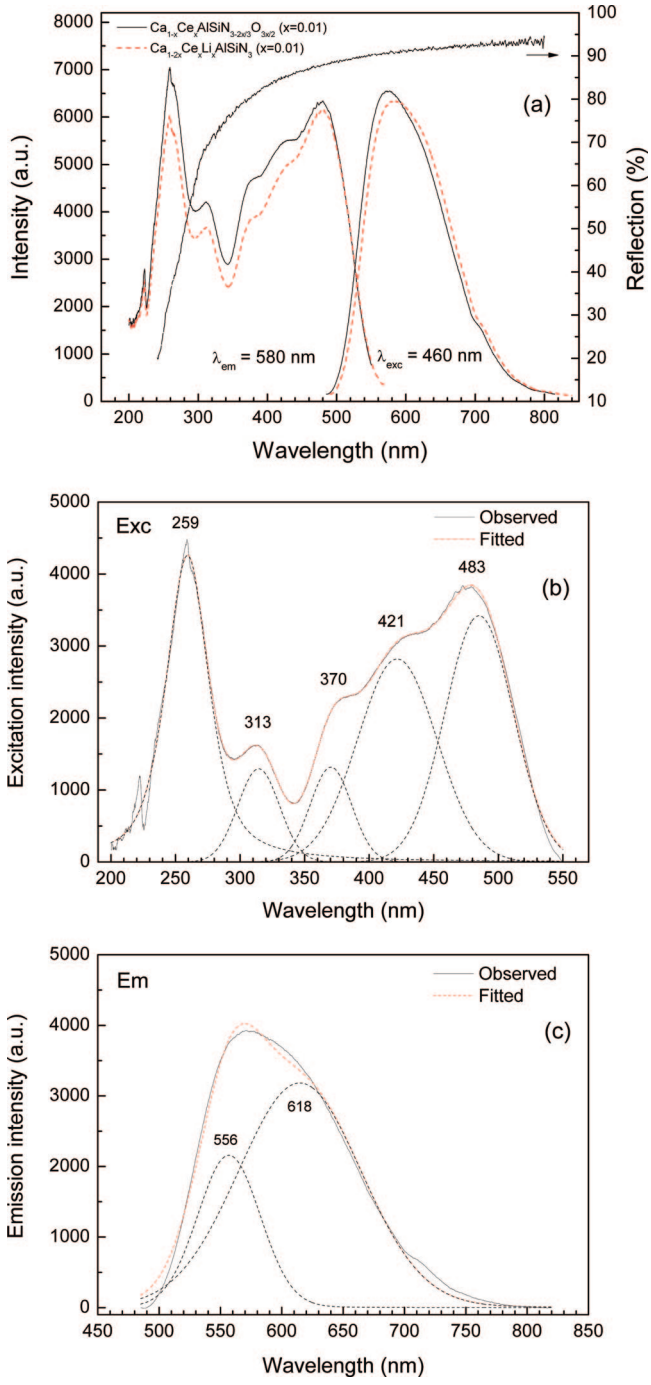

Figure 6. (a) Diffuse reflection spectrum of $CaAlSiN_3$ and excitation and emission spectra of $Ca_{1-2x}Ce_xLi_xAlSiN_3$ ($x = 0.01$) and $Ca_{1-x}Ce_xAlSiN_{3-2x/3}O_{3x/2}$ ($x = 0.01$); luminescence spectra of $Ca_{1-2x}Ce_xLi_xAlSiN_3$ ($x = 0.01$) with deconvolved Gaussian subbands for the excitation (b) and emission (c) spectra.

3.3. Luminescence Properties of $CaAlSiN_3:Ce^{3+}$. Figure 6a shows the reflection spectra of $CaAlSiN_3$ and the excitation and emission spectra of $Ca_{1-2x}Ce_xLi_xAlSiN_3$ ($x = 0.01$) and $Ca_{1-x}Ce_xAlSiN_{3-2x/3}O_{3x/2}$ ($x = 0.01$). There are two principle excitation bands: one is located under UV (200−330 nm) with a shoulder at about 310 nm and another one is in the visible spectral range (350−560 nm) with several subbands (or shoulders). The fundamental absorption edge of $CaAlSiN_3$ is estimated to be about 235 nm (5.3 eV) from its diffuse reflection spectrum, which is partial overlap with the top of the excitation band in UV. On the basis of the fact that the intensity of the UV excitation band peaking at about 258 nm can be varied by Ce concentration, this UV excitation band is really attributed to both the transitions from the valence to conduction bands of the host lattice of $CaAlSiN_3$ and from the 4f to 5d states of Ce^{3+}. Excitation under UV and/or blue spectral range, $CaAlSiN_3:Ce^{3+}$, emits efficient yellow-orange light with a maximum at around 580 nm for $x = 0.01$ having a slight variation with Ce concentration. In comparison with $Ca_{1-2x}Ce_xLi_xAlSiN_3$, the excitation and emission bands of $Ca_{1-x}Ce_xAlSiN_{3-2x/3}O_{3x/2}$ slightly shift to the blue spectral range along with an enhanced UV excitation band at ∼258 nm due to the incorporation of oxygen into the lattice. Moreover, both excitation and emission bands can be further decomposed into several Gaussian subbands (Figure 6b). As there is only one (Ca, Ce) site having a very low fivefold coordination number with nitrogen atoms within the range of 2.8 Å, a very stronger crystal field strength around (Ca, Ce) is expected. The excitation band of Ce^{3+} consists of up to five Gaussian components at about 259, 313, 370, 421, and 483 nm with a larger crystal field splitting (CFS) of the $4f^05d^1$ excited configure of Ce^{3+} of about 14 000 cm^{-1}. In addition, a lower center of gravity (COG), that is, the average energy of the excitation maxima of Ce^{3+} 5d states in the excitation spectrum, is observed of about 19 700 cm^{-1}, reflecting high covalent bonds of (Ca, Ce)−N (i.e., a larger nephelauxetic effect), which is much smaller than that in $Ca_2Si_5N_8:Ce^{3+}$ (∼22 300 cm^{-1}).[14] The emission band of $CaAlSiN_3:Ce^{3+}$ shows a broad nonsymmetrical band as expected for Ce^{3+}. Similarly, this emission band of Ce^{3+} can be fitted into two subbands peaking at about 556 nm (greenish-yellow) and 618 nm (red) roughly corresponding to the transitions of the 5d excited states to its two ground-state configurations of $^2F_{7/2}$ and $^2F_{5/2}$ of Ce^{3+}, respectively, with a difference of about 1800 cm^{-1} (in general ∼ 2000 cm^{-1} [27]), as shown in Figure 6c.

Exactly like in $CaAlSiN_3:Eu^{2+}$ [5,6] and in $M_2Si_5N_8:Eu^{2+}$ (M = Ca, Sr, Ba),[3] the position of the excitation band in the spectrum is nearly independent of Ce^{3+} in spite of the longest excitation band at about 480 nm (Figure 7), just showing a slight red-shift of about ≤6 nm, that is, 474−480 nm starting from $x = 0.001$ and stopping at $x = 0.02$ (Figure 7a), approximately corresponding to the changes of the lattice parameters of $Ca_{1-2x}Ce_xLi_xAlSiN_3$ (see section 3.2.), indicating that the maximum Ce solubility is at about $x = 0.02$. Meanwhile, as mentioned above, with the relaxation of the host lattice, in particular, the local structure, that is, the first nearest nitrogen atoms around (Ca, Ce, Li), the emission band of Ce^{3+} shifts toward longer wavelengths from 570 to 603 nm with increasing Ce concentration from $x = 0.001$ to 0.05, covering the yellow to orange spectral range. As the changes of both the CFS and COG are very limited in the whole Ce^{3+} concentration range, a red-shift of the emission band of Ce^{3+}, first, is ascribed to the Stokes shift (estimated from the longest excitation band and the first emission band at high energy by their decomposed excitation and emission spectra, respectively) mainly originating from the structural

(27) Blasse, G.; Grabmaier, B. C. *Luminescent Materials*: Springer-Verlag, Berlin, 1994.

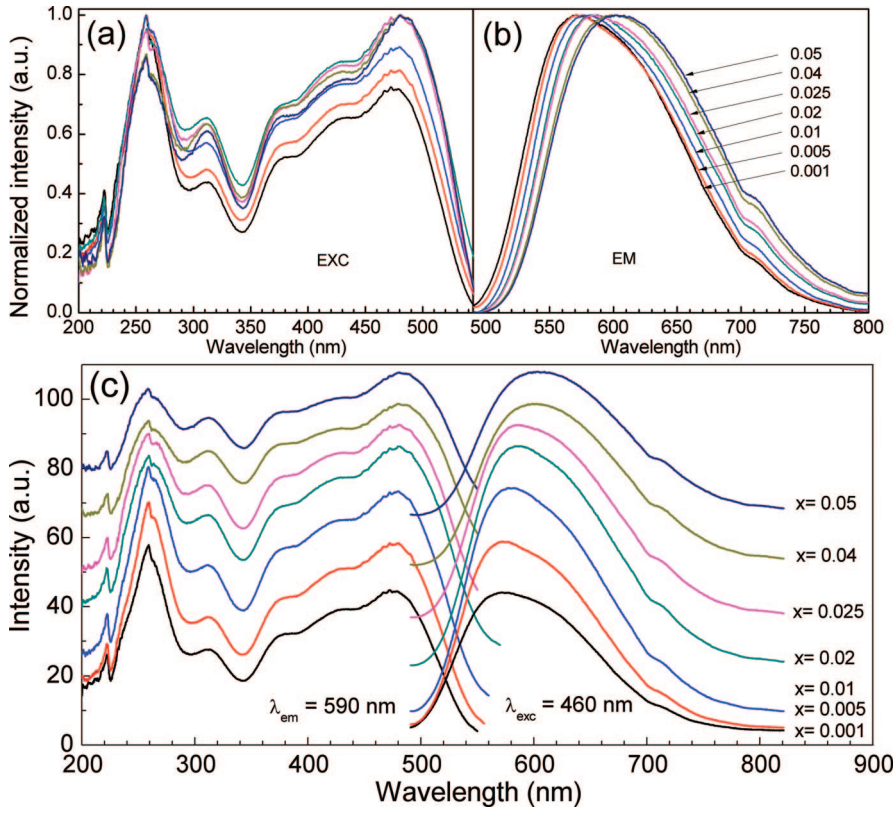

Figure 7. Excitation and emission spectra of $Ca_{1-2x}Ce_xLi_xAlSiN_3$; (a) and (b) are the normalized excitation and emission spectra.

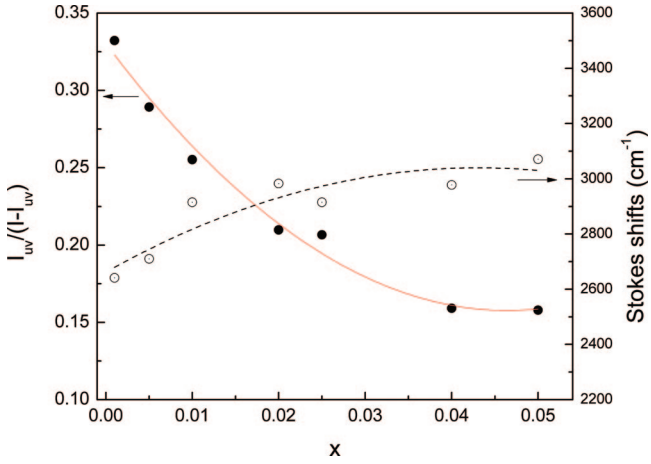

Figure 8. Ratio of the integrated excitation band under 260 nm to other excitation bands ($I_{uv}/(I - I_{uv})$) and the Stokes shift as a function of x in $Ca_{1-2x}Ce_xLi_xAlSiN_3$.

relaxation ranging from $x = 0.001$ to 0.02 (Figure 8) by which the emission band gradually shifts up to about 586 nm at $x = 0.02$ (with approximately about 14% increase of the Stokes shift). Second, energy transfer is also responsible for the red shift which probably can be classified into intra-Ce^{3+} (i.e., within one Ce^{3+} ion) and inter-Ce^{3+} (i.e., between $Ce^{3+}$and Ce^{3+} ions). With respect to energy transfer of intra-Ce^{3+}, namely, resonance reabsorption, the lower-lying 5d excitation levels of the crystal field splitting components of Ce^{3+}, particularly for the lowest energy level at ~480 nm, reabsorb the radiation light originating from the higher-lying 5d excitation energy levels, particularly for the highest energy level of ~260 nm. Evidently, this can be seen from the partial overlap between the excitation and the emission bands. As a consequence, the ratio of the integrated intensity of the top of the excitation band at 260 nm to those of the other four excitation bands decreases with increasing x (Figure 8), namely, $I_{uv}/(I - I_{uv})$, where I and I_{uv} are the integrated excitation area under total excitation curve and a band at 260 nm in the excitation spectra. Consistent with an increase of the Stokes shift, this kind of energy transfer is more effective at lower Ce concentrations with a significant decrease of $I_{uv}/(I - I_{uv})$, that is, higher reabsorption of lower-lying excitation levels, and then finally reaches a near constant at higher Ce concentrations (i.e., $x \geq 0.04$) due to the similar Stokes shift having the similar separations between the excitation and the emission bands in the spectra. Energy transfer is also observed occurring between Ce^{3+} and Ce^{3+}, say inter-Ce^{3+}, if Ce concentration is high enough. Especially at higher Ce concentrations, this kind of energy transfer is more possible with a shrinkage of the nearest distance of Ce−Ce; for example, the distance decreases from 3.2690(33) to 3.2128(24) Å with increasing x from 0.025 to 0.05 in $Ca_{1-2x}Ce_xLi_xAlSiN_3$. As a result, the emission band still can be shifted somewhat from 600 to 603 nm after $x = 0.04$, where the Stokes shift and reabsorption are believed to be already inactive. In this way, the profile/shape of the emission band of Ce^{3+} changes from the dominant transition from the 5d excitation states to high state configuration of $^2F_{5/2}$ of Ce^{3+} (see Figure 7c, $x < 0.025$) to the dominant transition of the 5d excitation states to low state configuration of $^2F_{7/2}$ of Ce^{3+} which shows the red-shift further.

As usual, the absorption of Ce^{3+} increases with increasing Ce concentration and reaches a saturation point of ~78% at about $x \geq 0.02$, also in good agreement with the estimated

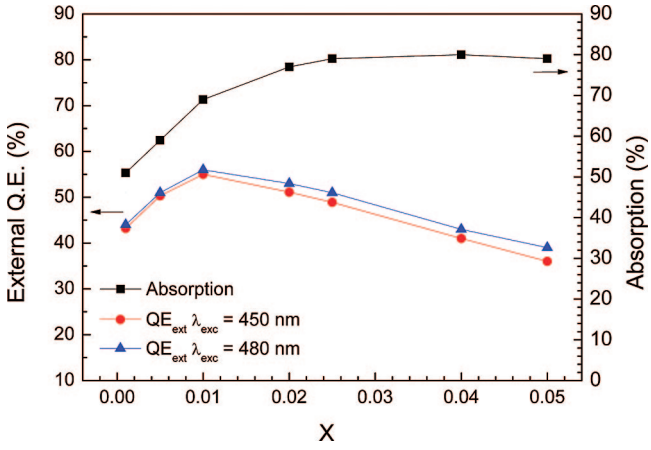

Figure 9. Absorption and external quantum efficiency (QE_{ext}) as a function of x in $Ca_{1-2x}Ce_xLi_xAlSiN_3$ under excitation at 450 and 480 nm, respectively.

Ce solubility limit for $Ca_{1-2x}Ce_xLi_xAlSiN_3$ (Figure 9). At low Ce concentration, with an increase of Ce^{3+} absorption the external quantum efficiency (QE_{ext}) of $Ca_{1-2x}Ce_xLi_xAlSiN_3$ increases as expected from $x = 0.001$ to 0.01 and reaches maximums of about 54% and 56% (with the absorption of 70%) at $x = 0.01$ under excitation at 450 and 480 nm, respectively. When $x > 0.01$, the external quantum efficiency significantly decreases caused mainly by Ce^{3+} concentration quenching, originating from the Ce−Ce interaction although the absorption of Ce^{3+} still can be increased up to $x = 0.025$ (Figure 9). In addition, as one $[CeLi]^{4+}$ pair substitutes two Ca^{2+} in the $CaAlSiN_3$ lattice and leaves one vacancy of Ca^{2+}, the absorbed energy cannot efficiently transfer to the Ce^{3+} ions but to the vacancies formed in the host lattice by the nonradiative ways. As a result, the external quantum efficiency and luminescence intensity decrease, in particular for higher Ce^{3+} concentrations due to more vacancies being expected. With a combination of the factors of the absorption, quantum efficiency, and formation of the defects, the optimal external quantum efficiency occurring at $x = 0.01$ probably can be explained. It is interesting to make a comparison with $CaAlSiN_3:Eu^{2+}$. The external quantum efficiency of $CaAlSiN_3$:Ce,Li is lower than that of $CaAlSiN_3:Eu^{2+}$ (~70% at λ_{exc} = 450 nm) due to a lower absorption of Ce^{3+} (70% at x = 0.01) versus Eu^{2+} (~84% at $x = 0.01$ in $Ca_{1-x}Eu_xAlSiN_3$). Furthermore, a higher conversion efficiency of Eu^{2+} is another possible reason as substitution Eu^{2+} for Ca^{2+} is 1:1 while Ce^{3+} for Ca^{2+} is 1:1.5, leaving a number of defects as the traps as discussed above in the host lattice and subsequently reducing the efficiency.

3.4. Thermal Stability of $CaAlSiN_3:Ce^{3+}$. Figure 10a plots the relative emission intensity of $Ca_{1-2x}Ce_xLi_xAlSiN_3$ ($x = 0.01$) and $Ca_{1-x}Ce_xAlSiN_{3-2x/3}O_{3x/2}$ ($x = 0.01$) as a function of temperature using a YAG:Ce^{3+} (P46-Y3) phosphor as a benchmark. The quenching temperature T_q (the temperature at which the emission intensity is half of the initial intensity at room temperature ~ 25 °C) for both materials is above 300 °C and is much higher than that of YAG:Ce^{3+} (P46−Y3, T_q=230 °C). Relatively, $Ca_{1-2x}Ce_xLi_xAlSiN_3$ ($x = 0.01$) has a higher thermal quenching rate than that of $Ca_{1-x}Ce_xAlSiN_{3-2x/3}O_{3x/2}$ ($x = 0.01$), which may account for an increased thermal ionization of Ce^{3+} at higher temperatures because of the Li^+ ion having a higher electron mobility, that is, the Li 2s2p energy levels could be partially bridging in between the 5d states of Ce^{3+} and the conduction band of $CaAlSiN_3$. In some of similar compounds first-principles calculations evidently indicate that the 2s2p states of Li are above 4.7 eV in $LiSi_2N_3$ and LiSiON, while the 3p state of Ca is located within about 3.7−5.6 eV and 3.5−5.75 eV which dominate the bottom of the conduction band of $CaAlSiN_3$[8] and $CaSiN_2$ (orthorhombic), respectively. As the relative emission intensities are above 87% and 64%, respectively, at 150 and 300 °C, which is comparable with $CaAlSiN_3:Eu^{2+}$, $Ca_{1-2x}Ce_xLi_xAlSiN_3$ ($x = 0.01$) and $Ca_{1-x}Ce_xAlSiN_{3-2x/3}O_{3x/2}$ ($x = 0.01$) are certainly suitable for use at high temperatures, in particular for white LED applications.

It should be noted that in order to achieve higher absorption and higher quantum efficiency, sufficient Ce concentration is prerequisite at the expense of a decrease of thermal stability. The thermal quenching rate of luminescence significantly increases with an increase of Ce concentration (corresponding to the quenching temperatures T_q decrease), as shown in Figure 10b. For lower Ce concentrations $x \leq 0.02$, the quenching temperature T_q is above 300 °C; however, the T_q is remarkably decreased in $Ca_{1-2x}Ce_xLi_xAlSiN_3$ when $x > 0.02$, for example 217 and 202 °C for $x = 0.04$ and 0.05, respectively. With raising temperature, in particular at higher Ce^{3+} concentrations, more thermal energy is available to excite electrons from the lowest 5d states of Ce^{3+} to the bottom of the conduction band of $CaAlSiN_3$ and then to be ionized, namely the thermal ionization processes,[27,28] by which the luminescence intensity/quantum efficiency is quenched due to an increased 5d electron concentration of Ce^{3+}. It is also observed that the emission band of Ce^{3+} exhibits a red shift for $x < 0.04$ and then a blue shift for $x > 0.04$ with increasing temperature at a fixed Ce concentration (Figure 10c). At lower Ce concentrations, the emission band of Ce^{3+} is mainly dominated by the transition of 5d → 4f (namely, intrinsic emission). Therefore, the structural relaxation (i.e., the lattice expansion) resulted by the temperature, just like the effect of the incorporation of Ce (see section 3.3), leads to the emission band shift to longer wavelengths probably also due to an increased Stokes shift. In contrast, at higher Ce concentrations ($x > 0.04$), as mentioned before, the position of the emission band is strongly related to the energy transfer of inter-Ce^{3+} which is strongly dependent on the nearest distance of Ce^{3+}−Ce^{3+}. Different from the 5d → 4f transition where the red-shift of the emission band mainly depends on the Stokes shift and the reabsorption apart from the CFS and COG effects, this red-shift of the Ce^{3+} emission from the energy transfer of inter-Ce^{3+} at room temperature is very unstable and degrades sharply at higher temperature due to an increased Ce−Ce distance, as found in $Sr_2Al_{2-x}Si_{1+x}O_{7-x}N_x:Eu^{2+}$.[29] In this way, the emission band in longer wavelength side is thermally quenched faster than that in shorter wavelength side. As a result, the emission band of Ce^{3+} shifts slightly toward shorter wavelength with raising

(28) Bol, A. A.; Meijerink, A. *Phys. Chem. Chem. Phys.* **2001**, *3*, 2105.
(29) Li, Y. Q.; Hirsaki, N.; Xie, R. J.; Mitomo, M. *Sci. Technol. Adv. Mater.* **2007**, *8* (7−8), 607.

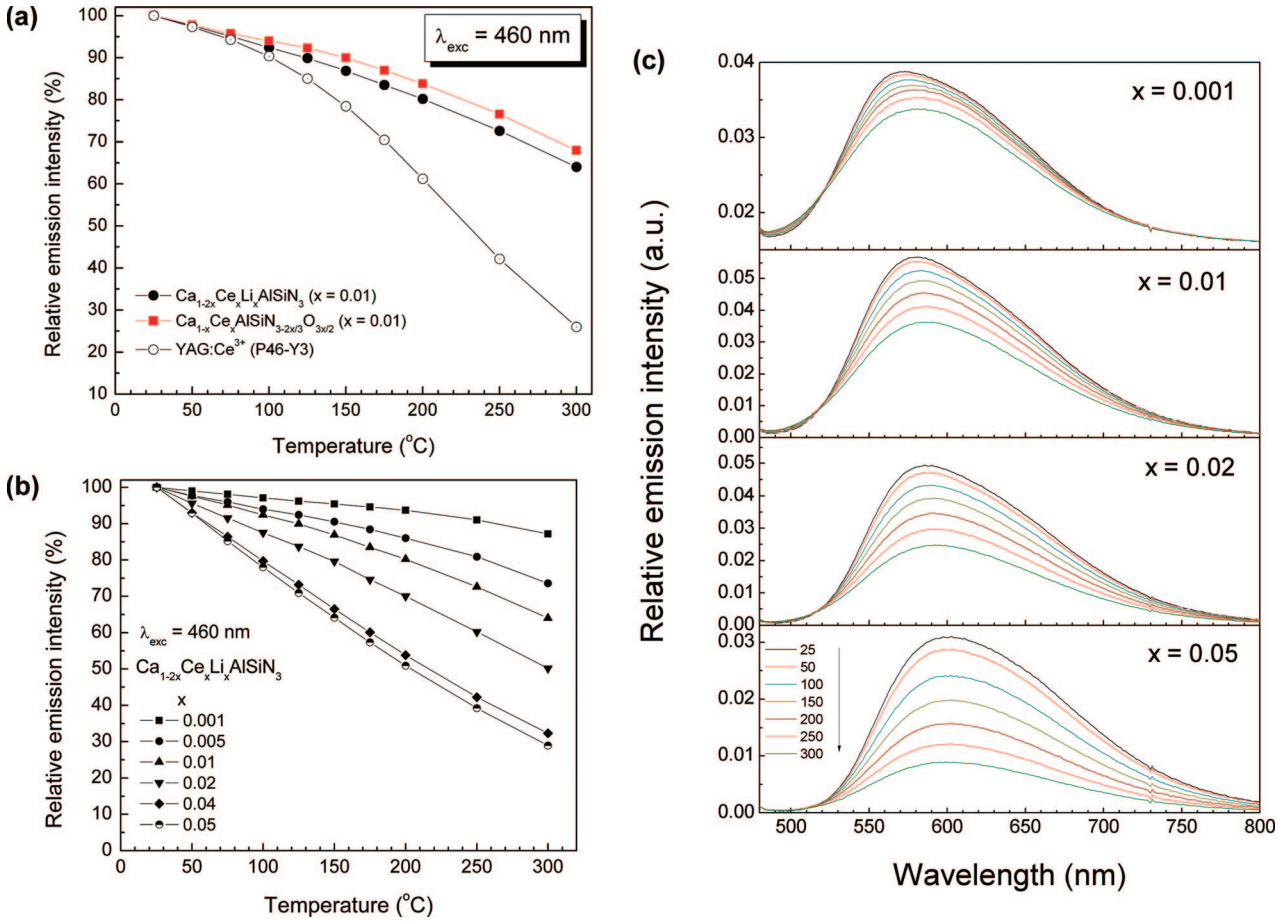

Figure 10. Temperature dependence of (a) $Ca_{1-2x}Ce_xLi_xAlSiN_3$ ($x = 0.01$) and $Ca_{1-x}Ce_xAlSiN_{3-2x/3}O_{3x/2}$ ($x = 0.01$) as well as YAG:Ce^{3+} (P46−Y3); (b) influence of the Ce concentration on the thermal quenching behaviors of $Ca_{1-2x}Ce_xLi_xAlSiN_3$; (c) emission spectra at different Ce concentration as a function of temperature in $Ca_{1-2x}Ce_xLi_xAlSiN_3$, under excitation at 460 nm.

the temperature until the position of intrinsic transition of 5d → 4f. On the basis of our work, in general, the emission band of Ce^{3+} or Eu^{2+} always shows a red-shift at first at lower Ce^{3+} or Eu^{2+} concentrations as a function of temperature and then transfers to a blue-shift at higher Ce^{3+} or Eu^{2+} concentrations. The critical concentration of such a transfer is dependent on M/Si or M/(Si, Al) ratio (e.g., metal/nonmetal ratio), where M is the alkaline earth or rare-earth metal ions.

Thermal stability of $Ca_{1-2x}Ce_xLi_xAlSiN_3$ ($x = 0.01$) as a function of aging time is depicted in Figure 11. Upon excitation at 460 nm, the emission of Ce^{3+} is very stable within 15 h at a fixed temperature of 200 °C under the relative humidity (RH) of 70% in air. The emission intensity is decreased only about 3.4% after 15 h with a very small blue-shift of the emission maxima, demonstrating that it is highly promising for white-light LED applications. In addition, a slight blue-shift of the emission band may be attributed to the oxidation of this material exposed in air during the aging, similar to the case of $Ca_{1-x}Ce_xAlSiN_{3-2x/3}O_{3x/2}$ (see Figure 6a).

3.5. Application in White LEDs. Since $CaAlSiN_3:Ce^{3+}$ can strongly absorb blue light and then efficiently convert the abosrbed primary blue light into yellow-orange light in the spectral range of 570−603 nm, similar to the cases of

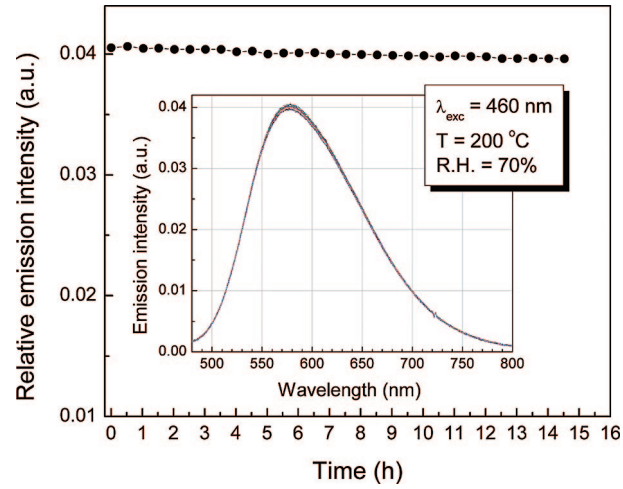

Figure 11. Thermal stability of $Ca_{1-2x}Ce_xLi_xAlSiN_3$ ($x = 0.01$) against the aging time at 200 °C under relative humidity 70% in air, $\lambda_{exc} = 460$ nm.

YAG:Ce^{3+}[30] and Ca-α-Sialon:Eu^{2+},[9,12,13,31] white LEDs can also be realized by single $CaAlSiN_3:Ce^{3+}$ phosphor embedded into a single blue LED chip (i.e., InGaN). Figure 12 illustrates the emission spectra of the obtained white LEDs

(30) Zukauskas, A.; Shur, M. S.; Gaska, R. *Introduction to Solid-State Lighting*; John Wiley & Sons, Inc.: New York, 2002.
(31) Sakuma, K.; Omichi, K.; Kimura, N.; Ohashi, M.; Tanaka, D.; Nirosaki, N.; Yamamoto, Y.; Xie, R.-J.; Suehiro, T. *Opt. Lett.* **2004**, *29*, 2001.

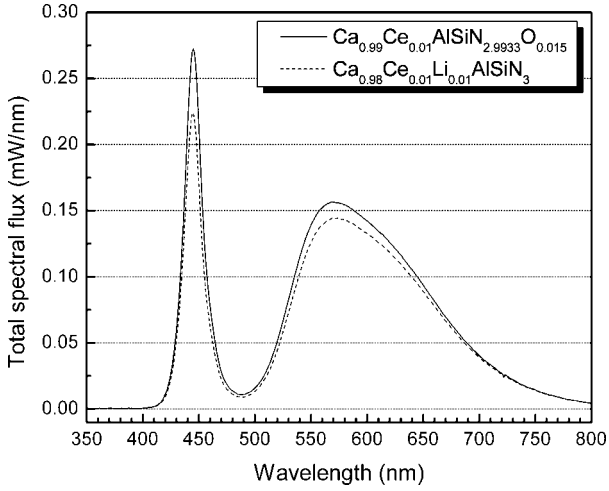

Figure 12. Emission spectra of white LEDs using $Ca_{1-2x}Ce_xLi_xAlSiN_3$ ($x = 0.01$) and $Ca_{1-x}Ce_xAlSiN_{3-2x/3}O_{3x/2}$ ($x = 0.01$) as the conversion phosphors.

Table 5. Optical Characteristics of White-LEDs with $CaAlSiN_3:Ce^{3+}$ as the Conversion Phosphors

material[a]	$Ca_{0.98}Ce_{0.01}Li_{0.01}AlSiN_3$	$Ca_{0.99}Ce_{0.01}AlSiN_{2.9933}O_{0.015}$
color point		
CIE x	0.389	0.377
CIE y	0.345	0.355
CCT (K)	3492	3722
CRI Ra	69.1	70.3
luminous efficacy (lm/W)	47	50.7

[a] CIE 1931. CCT: Correlated color temperature. CRI Ra: General color rendering index, average of R1 to R8.

of $Ca_{1-2x}Ce_xLi_xAlSiN_3$ ($x = 0.01$) and $Ca_{1-x}Ce_xAlSiN_{3-2x/3}O_{3x/2}$ ($x = 0.01$) with a combination of a blue LED chip (450 nm). As the typical examples, the main optical properties of $Ca_{1-2x}Ce_xLi_xAlSiN_3$ ($x = 0.01$) and $Ca_{1-x}Ce_xAlSiN_{3-2x/3}O_{3x/2}$ ($x = 0.01$) are summarized in Table 5. Comparable with white LED using a yellow emitting Ca-α-Sialon:Eu^{2+},[13] the obtained bichromatic white-light LEDs by the present work is also a high brightness warm white LED with a luminous efficacy of about 50 lm/W at a correlated color temperature of 3722 K, and the color rendering index (CRI Ra) is around 70. Of course, with the same problems of white LEDs using YAG:Ce^{3+} and Ca-α-Sialon:Eu^{2+} phosphors, the generated white-light LEDs with $CaAlSiN_3:Ce^{3+}$ phosphor lacks blue-green ($\sim$ 500 nm) and red ($\sim$ 630 nm) components in their emission spectrum. However, without doubt, it can be further improved by a way of blending $CaAlSiN_3:Ce^{3+}$ with other blue-green and red phosphors to make multichromatic white LEDs for widening the visible spectral range.

Finally, it is worth noting that the overall luminescence performance (i.e., PL intensity, external quantum, thermal quenching behavior, and the emission intensity of white-light LEDs) of $Ca_{1-x}Ce_xAlSiN_{3-2x/3}O_{3x/2}$ ($x = 0.01$) is slightly better than that of $Ca_{1-2x}Ce_xLi_xAlSiN_3$ ($x = 0.01$). The degradation in thermal stability at high temperature is understandable for the (Ce^{3+}, Li^+) codoped $CaAlSiN_3$ system due to the presence of Li^+ as discussed in section 3.4. With respect to the quantum efficiency and emission intensity for both phosphor and LEDs, apart from the synthetic process factors, the defect density in $Ca_{1-x}Ce_xAlSiN_{3-2x/3}O_{3x/2}$ probably is smaller than that in $Ca_{1-2x}Ce_xLi_xAlSiN_3$, and these defects are mainly formed at the anion sites (N or O) and not at the cation site like in $Ca_{1-2x}Ce_xLi_xAlSiN_3$. Therefore, $Ca_{1-x}Ce_xAlSiN_{3-2x/3}O_{3x/2}$ ($x = 0.01$) has good luminescence performance in comparison with that of $Ca_{1-2x}Ce_xLi_xAlSiN_3$ ($x = 0.01$). Fortunately, in fact, using sole CeO_2 instead of CeN and Li_3N as an activator is much more favorable for the production of $CaAlSiN_3:Ce^{3+}$ phosphor from practical viewpoints because CeO_2 is much cheaper, much more stable, and easier to handle than CeN and Li_3N.

4. Conclusions

(1) The crystal structure of $CaAlSiN_3$, prepared by a solid state reaction at 1700 °C under nitrogen atomsphere (0.48 MPa), has been improved. $CaAlSiN_3$ is found to be $CaAl_{1-4\delta/3}Si_{1+\delta}N_3$ ($\delta \approx 0.3 - 0.4$), in which the ratio of Al/Si is about 1/2.

(2) Ce^{3+} can be incorporated into the Ca^{2+} crystallographic site forming incomplete solid solutions of $Ca_{1-2x}Ce_xLi_xAlSiN_3$ and $Ca_{1-x}Ce_xAlSiN_{3-2x/3}O_{3x/2}$ with and without Li^+. The solubility limit of Ce^{3+} is about $x = 0.02$ for $Ca_{1-2x}Ce_xLi_xAlSiN_3$. Furthermore, Li^+ can increase the solubility of Al (i.e., a high Al/Si ratio). With increasing Ce content, the lattice parameters of $Ca_{1-2x}Ce_xLi_xAlSiN_3$ first slightly increase for $x \leq 0.02$ and then decrease due to a replacement of smaller Li^+ for large Ca^{2+}.

(3) $CaAlSiN_3:Ce^{3+}$ can efficiently absorb blue light in the spectral range of 450−480 nm and gives bright yellow-orange emission in the range of 570−603 nm. With increasing Ce concentration, the emission band of Ce^{3+} shows a red shift arising from the Stokes shift or structural relaxation and energy transfer at higher Ce concentrations. Excitation in the range of 450−480 nm, the absorption, and external quantum efficiency of $Ca_{1-2x}Ce_xLi_xAlSiN_3$ and $Ca_{1-x}Ce_xAlSiN_{3-2x/3}O_{3x/2}$ are about 70% and 56%, respectively, for $x = 0.01$.

(4) $CaAlSiN_3:Ce^{3+}$ has high thermal stability in the temperature range of 25−300 °C. The quenching temperature is greater than 300 °C at $x \leq 0.02$ but significantly decreases to 215 °C at $x \geq 0.04$ of $Ca_{1-2x}Ce_xLi_xAlSiN_3$ due to the thermal ionization of the 5d electrons of Ce^{3+} at the bottom of the conduction band of the host at high temperatures.

(5) Given a luminous efficacy of about 50 lm/W at color temperature of 3722 K as well as the color rendering index of 70 for the obtained warm white-LEDs, $CaAlSiN_3:Ce^{3+}$ demonstrates that it is a good yellow-orange phosphor for use in white-light LEDs.

Acknowledgment. We deeply thank Ms. Kazuko Nakajima for preparation of white-LEDs and measurement of their optical properties.

Supporting Information Available: Indexed powder XRD data (of $CeN_{0.97}$) (PDF). This material is available free of charge via the Internet at http://pubs.acs.org.

CM801669X